Electron Dynamics of Silicon Surface States: Second-Harmonic Hole Burning on Si(111) 7×7

John A. McGuire,[1] Markus B. Raschke,[2] and Y. Ron Shen[1]

[1]*Department of Physics, University of California at Berkeley, Berkeley, CA 94720, USA*
Materials Sciences Division, Lawrence Berkeley National Laboratory, Berkeley, California 94720
[2]*Max-Born-Institut für Nichtlineare Optik und Kurzzeitspektroskopie, D-12489 Berlin, Germany*

(Dated: June 8, 2005)

The ultrafast dynamics of electronic excitations of the surface dangling bond states of Si(111) 7×7 has been investigated by second harmonic generation as a probe of transient spectral hole burning. Spectral holes induced by a 100 fs pump at $\simeq 1.5$ eV and their decay are interpreted in terms of electronic dephasing times as short as 15 fs. This fast time scale together with the strong excitation-induced dephasing observed is interpreted in terms of carrier-carrier scattering. In addition, strong coupling of the electronic excitation to surface optical phonons is observed and attributed to the localization at adatom sites of a surface electronic excitation and a surface phonon mode.

PACS numbers: 78.47.+p,78.68.+m,73.25.+i,73.20.-r

The electron dynamics in solids determines the timescale and efficiency of charge and heat transport, charge screening [1, 2], and pathways for excited carrier relaxation [3]. When such processes occur at *surfaces*, they can control reaction pathways in surface photochemistry [4] and increasingly influence the performance of electronic and optoelectronic devices as their dimensions shrink [5]. Furthermore, on the nanoscale, surface electronic processes critically determine the optical behavior of metallic and semiconducting nanostructures due to their large surface-to-volume ratio [6].

Despite its importance, few studies have yet addressed the subpicosecond electron dynamics at surfaces [7–10]. In particular, with the coherent dynamics occurring on the timescale of just several tens of femtoseconds, its investigation remains challenging [9, 10]. An understanding of the evolution of the non-equilibrium electronic excitation, however, is highly desirable giving access to detailed understanding of the coupling mechanism between the electrons and between electrons and nuclear motions [3, 11]. For example, the confinement of surface electronic and vibrational wavefunctions is expected to yield much stronger electron-phonon coupling than is typically seen in three-dimensional structures.

The Si(111) surface with its 7×7 reconstruction provides a high-quality interface with low defect concentration. The associated dangling-bond states represent electronic states strongly localized in the surface normal direction. For these reasons Si(111)7×7 has served as a model system for surface chemistry [12], surface phase transitions [13] and transport studies [14]. However, little is known about the electronic dynamics at the Si(111)7×7 surface.

In this study we apply surface second-harmonic generation (SHG) as a probe of transient spectral hole burning, i.e., the surface-specific analogue of conventional bulk two-color pump-probe hole-burning spectroscopy. In this approach, the widths of the observed spectral holes in the nonlinear response of the surface correspond directly to the timescales of the electronic dephasing. The observed spectral holes correspond to electronic dephasing times as short as 15 fs and are characterized by strong excitation-induced dephasing. In addition, with the main spectral hole separated from the zero-phonon line by the surface LO-phonon frequency of 570 cm^{-1}, this implies a strong surface electron-phonon coupling between adatom electronic and vibrational modes.

The surface second-harmonic response can be expressed in terms of a local, dipolar second-order source polarization $\boldsymbol{P}^{(2)}(2\omega) = \chi^{(2)}(2\omega;\omega)\mathbf{E}(\omega)\mathbf{E}(\omega)$ [15, 16], where $\chi^{(2)}$ denotes the surface nonlinear susceptibility. In the surface-specific implementation of spectral hole burning, we measure the SHG from a probe beam as a function of detuning relative to the pump beam at a fixed wavelength. The second-harmonic of this probe pulse is then generated by a nonlinear susceptibility $\chi^{(2)}(2\omega_{\rm pr};\omega_{\rm pr};\omega_{\rm pu})$ that has been modified by the pump pulse [15, 16].

In the vicinity of the fundamental pump photon energy of 1.54 eV chosen in our experiments, the SHG response of Si(111)7×7 is characterized by two spectral features as shown in Fig. 1 [17, 18]. As indicated schematically, the broad low-energy peak has been identified with a one-photon transition from the silicon rest atom S_2 into the adatom U_1 dangling-bond surface states [17, 18]. In contrast, the feature at a fundamental photon energy of 1.7 eV can be attributed to a two-photon resonance at 3.4 eV [17], which corresponds to the energy of the bulk E_1 transition and the energy between back-bond bonding S_3 and anti-bonding U_2 states.

The dangling bond (db) contribution $\chi^{(2)}_{\rm res,0}(2\omega_{\rm pr};\omega_{\rm pr})$ to the total surface nonlinear susceptibility $\chi^{(2)}$ can be expressed by a single resonant term due to a pair of surface states $|a\rangle$ and $|b\rangle$ (i.e., a resonance with $\omega_{\rm pu} \sim \omega_{\rm pr} \sim \omega_{ba}$). The large width of this db resonance suggests that it is inhomogeneously broadened. The two-photon resonance at about 3.4 eV as well as any weak, completely non-resonant contributions are summarized by an effective nonresonant contribution $\chi^{(2)}_{\rm NR}(2\omega_{\rm pr};\omega_{\rm pr})$, which we consider as unaffected by the pump as discussed below. Experimentally, a strictly sequential pump-probe sequence is employed to avoid coherent artifacts. Then, in analogy to the case of bulk hole-burning spectroscopy, in the presence of a static inhomogeneous distribution $g(\omega_{ba})$ of res-

onant frequencies much broader than the homogeneous line width Γ_{ba}, $\chi^{(2)}$ can be expressed as

$$\chi^{(2)}(2\omega_{pr};\omega_{pr};\omega_{pu}) = \chi^{(2)}_{NR}(2\omega_{pr};\omega_{pr}) + \chi^{(2)}_{res,0}(2\omega_{pr};\omega_{pr}) \times \left\{1 - i\frac{I}{I_s}\frac{\Gamma_{ba}}{\Delta + i2\Gamma_{ba}}\right\}, \quad (1)$$

where $\Delta = \omega_{pr} - \omega_{pu}$, $\chi^{(2)}_{res,0}(2\omega_{pr};\omega_{pr})$ is the effective db nonlinear susceptibility in the absence of the pump beam, and I and I_s are respectively the pump intensity and the saturation pump intensity [16]. The short timescales for incoherent population redistribution of a non-equilibrium electronic distribution in condensed systems require the hole-burning measurements to be performed transiently.

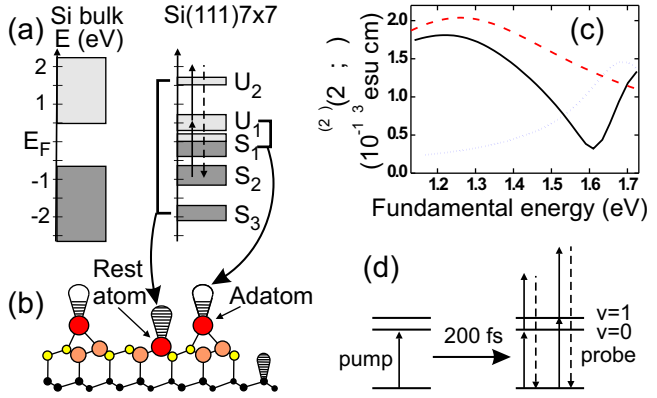

FIG. 1: (a) Surface-projected silicon bulk and surface band structure with adatom (S_1 and U_1) and rest-atom (S_2) dangling-bond and adatom-back-bond (S_3 and U_2) surface states. (b) Ball-and-stick model of surface atoms indicating localized dangling bond electrons. (c) SHG spectra for clean (solid curve) and hydrogen-terminated (dotted curve), i.e., dangling bond quenched, Si(111)7×7 (after [17, 18]) and dangling-bond contribution (dashed curve) to the nonlinear susceptibility. (d) Three-level model for the S_2 to U_1 one-photon resonance discussed in the data analysis.

The experiments were performed in an ultrahigh vacuum (UHV) chamber with a base pressure of $< 8\times10^{-11}$ mbar. Samples were cut from wafers of single-crystal, p-doped (1 − 2 Ω cm) Si and mounted on a liquid-nitrogen-cooled sample holder with the $[2\bar{1}1]$ crystallographic axis oriented perpendicularly to the optical plane. As verified by low-energy electron diffraction (LEED) and Auger electron spectroscopy (AES), clean and well ordered Si(111)7×7 surfaces were prepared following established procedures [17].

The pump pulses were taken from a Ti:sapphire oscillator/regenerative-amplifier system producing 1 mJ, 100 fs pulses at $\lambda = 805$ nm at a repetition rate of 1 kHz. Frequency doubling of the output of a β-BaB_2O_4-based continuum-seeded optical parametric amplifier [19] provided the probe beam. The pump and probe pulses each had a bandwidth of ~ 200 cm^{-1}. To ensure uniform pumping, the probe beam was focussed to a diameter ~ 25 % of that of the pump. As shown schematically in the inset of Fig. 2(a) the pump and probe beams were incident respectively at 47° and 43° with respect to the sample normal. The fluences at the sample surface were alternately set to 200, 400, 800, and 1600 μJ/cm^2 for the pump and about 100 μJ/cm^2 for the probe beam. Transit-time differences of the two beams across the beam spot on the surface effectively reduced the temporal resolution to about 200 fs. With the input pump, probe, and SHG output being *p*-, *s*-, and *s*-polarized, respectively, the anisotropic nonlinear susceptibility tensor element $\chi^{(2)}_{\parallel\parallel\parallel}$ was probed [15, 16].

The resulting two-color pump/SHG-probe scans shown in Fig. 2 display a rapid, pump-induced decrease of the probe SHG signal. The subsequent recovery of the probe SHG signal on a timescale of several hundred fs provides the timescale of the relaxation of the excited- and ground-state population difference (inelastic scattering). The recovery of both negative- and positive-detuning data can be fit with single exponentials within the first several ps with recovery times of 730 ± 160 fs and 490 ± 90 fs, respectively.

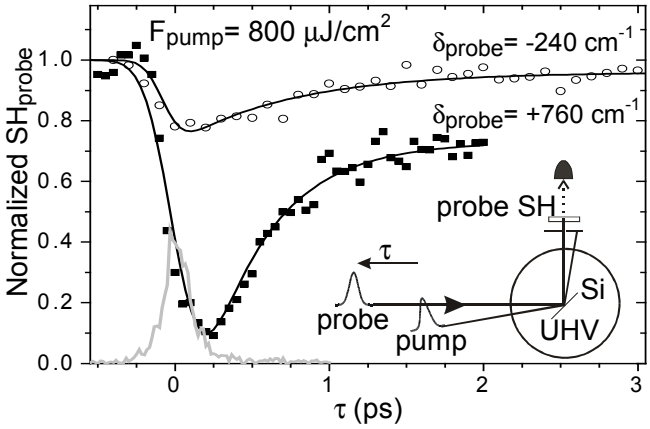

FIG. 2: Pump-SH_{probe} scans for probe-pump detunings $\hbar\omega_{pr} - \hbar\omega_{pu}$ of -29 meV (open circles) and -93 meV (filled squares) at a pump fluence of 800 μJ/cm^2. Data are normalized to the SHG signal at a probe delay of -500 fs. The solid lines serve as guides to the eye. The gray curve describes the sum-frequency cross-correlation between pump and probe pulses. Inset: schematic of the experimental layout.

The probe SHG is the result of an interference between the resonant dangling-bond contribution $\chi^{(2)}_{res}(2\omega_{pr};\omega_{pr})$ and the effective nonresonant contribution $\chi^{(2)}_{NR}(2\omega_{pr};\omega_{pr})$. In order to extract the spectral-hole data for the dangling-bond excitations only, the relative phases and magnitudes between $\chi^{(2)}_{res}$ and $\chi^{(2)}_{NR}$ have been determined [22]. Figure 3 shows the resulting spectral hole induced by the dangling-bond excitation observed at a probe delay of 200 fs. As is particularly evident from the low-fluence data, the results are characterized by a comparably weak hole at zero detuning followed by a second, more pronounced hole several hundred wavenumbers to higher energies. The data can be fit using a modified version of Eq. (1) that models the effect of the pump as a pair of spectral holes at probe-pump detunings of $\delta = 0$ and

TABLE I: Parameters for the two Lorentzian holes in Eq. 2 used to fit the data for the pump-induced holes in Fig. 3 with $\delta = 570\ \mathrm{cm}^{-1}$.

Fluence [μJ/cm^2]	A_F [cm^{-1}]	Γ_F [cm^{-1}]	A'_F [cm^{-1}]	Γ'_F [cm^{-1}]
1600	23 ($\pm^{71}_{23}$)	450 (340)	364 (160)	380 (70)
800	80 (10)	255 (30)	100 (10)	120 (20)
400	34 (5)	170 (15)	90 (10)	100 (10)
200	16 (3)	115 (25)	60 (5)	80 (10)

$\delta = 570 \pm 100\ \mathrm{cm}^{-1}$:

$$\chi^{(2)}(2\omega_{pr};\omega_{pr};\omega_{pu}) = \chi^{(2)}_{NR}(2\omega_{pr};\omega_{pr}) + \chi^{(2)}_{res,0}(2\omega_{pr};\omega_{pr}) \times \{1 - i2\pi A_F/(\Delta + i4\pi\Gamma_F) - i2\pi A'_F/(\Delta - 2\pi\delta + i4\pi\Gamma'_F)\}. \quad (2)$$

The fit values of the parameters are given in Table I. The fit was restricted to $\omega_{pr} - \omega_{pu} < 2\pi \cdot 750\,\mathrm{cm}^{-1}$, because at larger detunings the pump-probe trace appeared qualitatively different from those in Fig. 2, suggesting that other pumped excited state must have also contributed to the observed SHG.

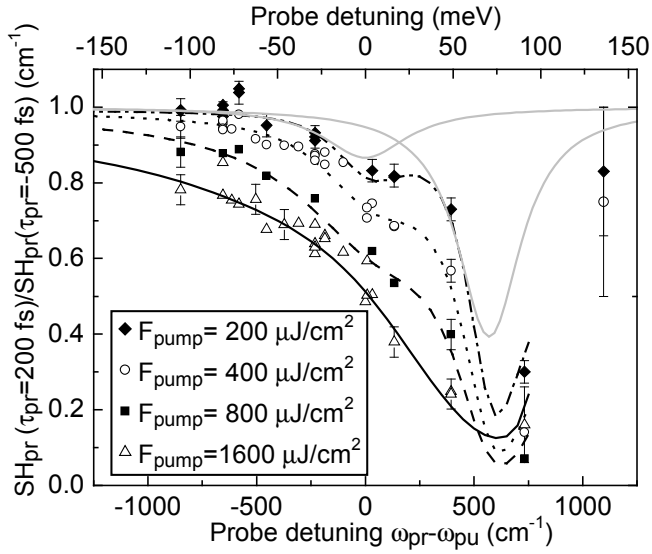

FIG. 3: Measured values of $\mathrm{SH}_{pr}(\tau_{pr} = 200\,\mathrm{fs})/\mathrm{SH}_{pr}(\tau_{pr} = -500\,\mathrm{fs})$ versus probe detuning at several pump fluences. The curves are fits to Eq. (2) using the parameters of Table I and the experimentally measured relative magnitudes and phases of $\chi^{(2)}_{res,0}$ and $\chi^{(2)}_{NR}$. The gray curves show the individual spectral holes from Eq. (2) for the case of $F_{pump} = 200\ \mu J/\mathrm{cm}^2$.

As seen in Table I, the fitted values of Γ_F depend on pump fluence. The contribution of saturation broadening to Γ_F was estimated to be less than $\sim 10\%$ at the highest pump fluence. The width of the zero-detuned hole shows a linear dependence on pump fluence and translates into a homogeneous dephasing time of the order of tens of femtoseconds as indicated in Fig. 4, in which the rates have been corrected for contributions from the pump and probe linewidths. Extrapolation to zero pump fluence yields an intrinsic homogeneous dephasing time of ~ 100 fs.

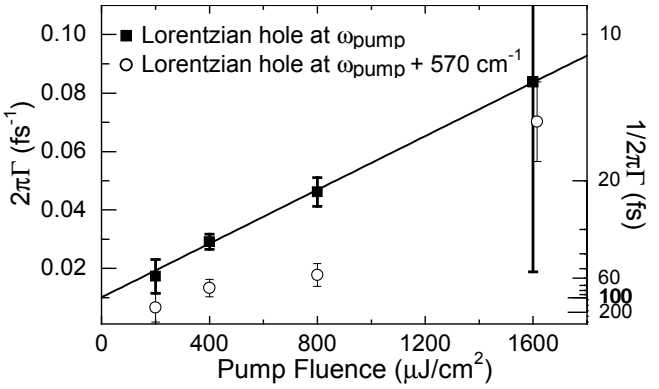

FIG. 4: Homogeneous dephasing rates deduced from the two-Lorentzian fit of the data versus pump fluence. Extrapolation to zero pump fluence yields an intrinsic homogeneous dephasing time of ~ 100 fs.

The observation of the deep hole at probe-pump detuning of 570 cm^{-1} implies strong coupling between the excited adatom electronic state and the 570 cm^{-1} surface optical phonon of Si(111)7×7 [23]. Such coupling can be explained in terms of the localization of both electronic and phonon modes at the adatoms. The adatom electronic bands are weakly dispersive [24, 25], and STM measurements show that the density of states associated with the unoccupied adatom-dangling-bond band U_1 is largely localized to the adatom positions in the 7×7 unit cell [26]. Likewise, the optical phonon mode at 570 cm^{-1} is identified with the out-of-plane motion of the adatoms and the Si atoms immediately below the adatoms along the surface normal and against each other [23]. The degree of localization of the electronic and vibrational modes associated with the adatoms, although perhaps not as pronounced as in molecular systems, exceeds what one would expect for a two-dimensional system that is confined in one direction but very delocalized in the plane. Thus, electron transfer from the adatoms to the rest atoms at the Si(111)7×7 surface could allow for a strong Fröhlich contribution to the electron-phonon coupling. The absence of a phonon sideband at a probe detuning of -570 cm^{-1} can be understood by noting that the initial state for the one-photon resonance in our measurements is associated with the rest atoms, which are not expected to be coupled to phonon modes associated with the adatoms, and that at a temperature of 80 K, the thermal population of phonons at 570 cm^{-1} is small ($n_{phonon} = 4 \times 10^{-5}$). Therefore, the one-phonon transitions expected in this system are as shown in Fig. 1(d) with the lower excited state being an excitation of the adatom dangling bond and the upper excited state being an excitation of the adatom dangling bond along with coherent excitation of an optical phonon at 570 cm^{-1}. However, in general and due to the fact that the spectral hole at positive detuning is deeper than the central hole, it can not be excluded that, e.g., Coulombic coupling of the db excitation to the backbond resonance contributes to the observed spectral response.

The deduced intrinsic homogeneous dephasing time of $\sim$

100 fs can be compared with measurements of the homogeneous dephasing rates in the range of 20 to 30 fs determined for surface or image-potential states of Cu(111) [9, 27]. For the silicon surface, the lower carrier-charge density would lead one to expect longer dephasing times as observed here. Interestingly, the odd number of electrons in the Si(111)7×7 unit cell and the non-zero electron density in the vicinity of the surface Fermi energy suggest that the Si(111)7×7 surface may in fact be metallic [24]. Despite that, however, the electron density in any conduction band at the Si(111)7×7 Fermi surface is considerably lower than in Cu(111).

The short timescales of homogeneous dephasing derived from our hole-burning spectra are consistent with the results from the transient grating experiments of Voelkmann *et al.* on Si(111)7×7 [10]. At a fluence of about 400 μJ/cm^2, as used in their experiment, our value for the homogeneous dephasing time of about 40 fs would result in a photon echo decay time constant of about 10 fs, shorter than the 14 fs pulse length used in their measurements.

Such rapid dynamics can arise from only a limited number of mechanisms. The density of defects normally required to produce rapid dephasing [28, 29] far exceeds the number expected on clean Si(111)7×7. A time-resolved two-photon photoemission study of carrier dynamics on Si(100)$c(4\times 2)$ suggests that optical-phonon emission via deformation-potential scattering of excited db electrons can occur on a timescale of $\sim$ 300 fs [7], but it cannot account for the linear dependence of the dephasing time on the pump fluence observed here (Fig. 4). The latter observation suggests that carrier-carrier scattering is the dominant dephasing mechanism in the regime of higher pump energies. For example, as observed in studies of hole decoherence on Cu(100), Auger recombination can occur within tens of fs [9]. Similarly, ultrafast photon-echo measurements in GaAs-GaAlAs quantum-well structures yielded homogeneous dephasing times decreasing from 200 to 64 fs with increasing excitation density [2].

Carrier-carrier scattering might also be a significant contribution to the intrinsic homogeneous dephasing rate. Even in the limit of a single photoexcited electron-hole pair in the U_1 and S_2 bands respectively, there are still electrons at or near the Fermi level in the adatom-derived S_1 band. These electrons could account for rapid scattering of coherently excited carriers. However, as suggested by the photoemission results cited above as well as our evidence for strong electron-phonon coupling, scattering with phonons must play an important role in the zero-fluence dephasing.

In summary, our results offer insight into both ultrafast carrier-carrier interactions and electron-phonon coupling on Si(111)7×7. In order to derive the full dynamics of the system, measurements of the spectral diffusion are desirable. To arrive at a more detailed understanding, a more precise knowledge of the Si(111)7×7 surface band structure is needed and many-body and correlation effects have to be considered.

The authors acknowledge insightful discussions with Klaus Reimann and Michael Wörner. This work was supported by the Director, Office of Science, Office of Basic Energy Sciences, Materials Sciences and Engineering Division, of the U.S. Department of Energy under Contract No. DE-AC03-76SF00098.

[1] W. Knox *et al.*, Phys. Rev. Lett. **61**, 1290 (1988);
[2] J.-Y. Bigot *et al.*, Phys. Rev. Lett. **67**, 636 (1991).
[3] Z. Wang *et al.*, Phys. Rev. Lett. **94**, 037403 (2005).
[4] D. Denzler *et al.*, Phys. Rev. Lett. **91**, 226102 (2003).
[5] L. Reggiani, *Hot Electron Transport in Semiconductors* (Springer, New York, 1985).
[6] M. Nirmal *et al.*, Nature **383**, 802 (1996).
[7] M. Weinelt *et al.*, Phys. Rev. Lett. **92**, 126801 (2004).
[8] N.H. Ge *et al.*, Science **279**, 202 (1998). C.B. Harris *et al.*, Annu. Rev. Phys. Chem. **48**, 711 (1997).
[9] H. Petek, H. Nagano, and S. Ogawa, Phys. Rev. Lett. **83**, 832 (1999). H. Petek and S. Ogawa, Prog. Surf. Science **56**, 239 (1997).
[10] C. Voelkmann *et al.*, Phys. Stat. Sol. a **175**, 169 (1999). C. Voelkmann *et al.*, Phys. Rev. Lett. **92**, 127405 (2004).
[11] C. H. B. Cruz *et al.*, Chem. Phys. Lett. **132**, 341 (1986).
[12] H. N. Waltenburg and J. J. T. Yates, Chem. Rev. **95**, 1589 (1995). F. Tao and G. Xu, Acc. Chem. Res. **37**, 882 (2004).
[13] A. Mascaraque and E. Michel, J. Phys.: Cond. Matt. **14**, 6005 (2002).
[14] T. Tanikawa *et al.*, Phys. Rev. Lett. **93**, 016801 (2004).
[15] T. Heinz, in *Nonlinear Surface Electromagnetic Phenomena*, edited by H.-E. Ponath and G. Stegeman (Elsevier Science Publishers B.V., Amsterdam, 1991).
[16] Y. Shen, *The Principles of Nonlinear Optics* (John Wiley & Sons, Inc., New York, 1984).
[17] U. Höfer, Appl. Phys. A **63**, 533 (1996).
[18] T. Suzuki, Phys. Rev. B **61**, R5117 (2000).
[19] R. Kaindl *et al.*, J. Opt. Soc. Am. B **17**, 2086 (2000).
[20] M. Yilmaz, A. Rajagopal, and F. Zimmermann, Phys. Rev. B **69**, 125413 (2004).
[21] G. A. Schmitt *et al.*, in preparation.
[22] This was achieved by selective quenching of the db contribution to $\chi^{(2)}_{\rm res}$ by H adsorption assuming that the magnitude and phase of $\chi^{(2)}_{\rm NR}$ are unaffected by H adsorption [17, 20, 21]. For fundamental wavelengths from 760 nm to 920 nm, the complex quantity $\chi^{(2)}_{\rm res,0}/\chi^{(2)}_{\rm NR} = R\exp(i\phi_{\rm NR})$ could be well fit by the polynomial forms $\phi_{\rm NR} = 160^\circ - 0.008\,\delta + 1.1\times10^{-5}\,\delta^2 - 2.1\times10^{-8}\,\delta^3 - 3.4\times10^{-11}\,\delta^4 - 1.2\times10^{-14}\,\delta^5$ and $R = 2.9 - 9\times10^{-4}\,\delta + 1.6\times10^{-6}\,\delta^2 - 1.4\times10^{-9}\,\delta^3 - 2.6\times10^{-12}\,\delta^4 - 8\times10^{-16}\,\delta^5$, for $\lambda_{\rm pr} < 864$nm and $R = 4.1 - 6\times10^{-4}\,\delta$, for $\lambda_{\rm pr} > 864$nm, where $\delta = \nu_{\rm pr} - 12500{\rm cm}^{-1}$ – consistent with measurements by Schmitt *et al.* [21].
[23] W. Daum, H. Ibach, and J. Müller, Phys. Rev. Lett. **59**, 1593 (1987). J. Kim *et al.*, Phys. Rev. B **52**, 14709 (1995).
[24] R. Losio, K. N. Altmann, and F. J. Himpsel, Phys. Rev. B **61**, 10845 (2000).
[25] J. Ortega, F. Flores, and A. L. Yeyati, Phys. Rev. B **58**, 4584 (1998).
[26] R. J. Hamers, R. M. Tromp, and J. E. Demuth, Phys. Rev. Lett. **56**, 1972 (1986).
[27] E. Knoesel, A. Hotzel, and M. Wolf, J. Electron Spec. Relat. Phenom. **88**, 577 (1998).
[28] M. Weinelt *et al.*, Appl. Phys. B **68**, 377 (1999).

[29] M. Roth *et al.*, Phys. Rev. Lett. **88**, 096802 (2002).